

Discovery of polymetallic porphyry at the Silver Queen, British Columbia using airborne EM and TITAN-24 DCIP and MT surveys

Nasreddine Bournas¹, Ellen Clements², and Rob Hearst³

Abstract

Airborne electromagnetic, ground direct current and induced polarization (DCIP), and magnetotelluric (MT) surveys have extensively been used in mining exploration and more particularly for the exploration of base metal mineralization. The continuous development of geophysical techniques with advances in the instrumentation and signal processing and the recent development of robust 3D inversion algorithms make possible the detection and accurate delineation of deep-seated mineralization of economic interest. Recently, a deep-penetrating TITAN-24 DCIP and MT survey was conducted over the Silver Queen project area, located in British Columbia, Canada in two phases (2011 and 2012, respectively) by Quantec Geoscience Ltd. on behalf of New Nadina Explorations Ltd. for the exploration of porphyry-style polymetallic mineralization. The ground survey was carried out as a follow-up to the helicopter-borne *z*-axis tipper electromagnetic survey flown during the spring of 2011 by Geotech Ltd. with the aim to delineate favorable areas for the exploration of porphyry-style deposits. A deep-seated significant zone of anomalously high chargeability occurring in coincidence with a conductive zone was detected by the ground DCIP and MT survey. Drill-testing based on the 3D inversion results of the data led to the discovery of a new significant deep-seated porphyry-style mineralization. The discovery drillhole contained visible disseminated to semimassive sulphide mineralization, gold and molybdenite over 350 m for a total drillhole depth of approximately 800 m and occurs in association with a significant mineralized stockwork zone open at depth.

Introduction

The Silver Queen is a polymetallic vein-type mineralized zone, located 35 km southeast of Houston, British Columbia, Canada that has been the focus of various exploration programs over the last century to discover the anticipated stockwork style deposit thought to be genetically associated with the observed near-surface mineralized veins. A deep-penetrating TITAN-24 direct current and induced polarization (DCIP) and magnetotelluric (MT) survey was recently carried out over the Silver Queen project area, in two phases (2011 and 2012) by Quantec Geoscience Ltd. on behalf of New Nadina Explorations Ltd. for the exploration of porphyry-style polymetallic mineralization (Bournas et al., 2012). The ground survey was conducted as a follow-up to the helicopter-borne *z*-axis tipper electromagnetic (ZTEM) survey flown during the spring of 2011 by Geotech Ltd. (Kowalczyk and van Kooten, 2011) and previous geologic mapping surveys conducted by Leitch et al. (1990).

In this paper, we present the 3D inversion results and an interpretation of the data obtained from the airborne ZTEM and the ground TITAN-24 DCIP and MT surveys, which have led to the discovery of the Itsit porphyry-

style mineralized stockwork. The ZTEM helicopter-borne electromagnetic (EM) and magnetic survey, which was carried out as a mapping tool, was very successful in mapping and detecting known and new faults associated with zones of alteration and brecciation and was particularly useful in delineating geologic structures associated with various volcanic and intrusive rocks, which were evident as resistivity and magnetic susceptibility contrasts, and as zones of low or high magnetic response and low or high resistivity signature. The ground follow-up conducted with the TITAN-24 DCIP and MT system in the central area of the Silver Queen property led to the discovery of a new significant porphyry-style mineralization confirmed by the recent drilling results. These results have provided evidence of the existence of deep-seated mineralization associated with a new stockwork deposit. Mineralization consists mainly of copper, gold, and good grades of molybdenum and is associated with a significant stockwork body (Hutter, 2011).

Geology and mineralization of the Silver Queen

The Silver Queen project area is located in the Bulkley Valley region of Central British Columbia. On a

¹Formerly Quantec Geoscience Ltd., Canada; presently Geotech Ltd., Canada. E-mail: nbournas@bell.net.

²New Nadina Explorations Ltd., Canada. E-mail: nadina2005@shaw.ca.

³Areva Resources Canada Inc., Canada. E-mail: robert.hearst@areva.ca.

Manuscript received by the Editor 28 March 2013; published online 2 August 2013. This paper appears in INTERPRETATION, Vol. 1, No. 1 (August 2013); p. T101–T112, 9 FIGS.

<http://dx.doi.org/10.1190/INT-2013-0044.1>. © 2013 Society of Exploration Geophysicists and American Association of Petroleum Geologists. All rights reserved.

regional scale, this area lies within a resurgent caldera rim of the Buck Creek basin. This feature is roughly delineated by a series of rhyolite outliers and semi-circular alignment of Upper Cretaceous and Eocene volcanic complex (McIntyre, 1985). The oldest rocks known in the basin area belong to the Jurassic Hazelton Group. Large areas of younger Upper Cretaceous rocks consisting of lower acidic volcanic formations are exposed eastward of the Owen Lake area, where they host the Silver Queen deposit. The Upper Cretaceous rocks are in turn overlain by the Eocene Ootsa Lake Group, which includes the Goosly Lake andesitic and trachyandesitic volcanic rocks and the Buck Creek andesitic to dacitic volcanic formations. Basaltic formations of the Upper part of the Buck Creek formations belong to the Endako Group of the Eocene-Oligocene age as shown on the map in Figure 1 (McIntyre, 1985).

Locally, the geology of the Silver Queen area is subdivided into five major units and three dike types (Leitch et al., 1990), as shown in Figure 2. A basal reddish polymictic conglomerate (unit 1) is overlain by fragmental rocks including a thick crystal tuff (unit 2), coarse lapilli tuff and breccias (unit 3), overlain by a thick feldspar-porphyrific andesite flow unit (unit 4), intruded by microdioritic sills and other small intrusions (unit 5). The stratified formations form a gently north-west-dipping succession, with the oldest rocks exposed near Riddeck Creek to the south and the youngest exposed in Emil Creek to the north. All these units are cut by dikes that can be divided into three groups: amygdaloidal dikes (Unit 6), bladed feldspar porphyry dikes (Unit 7), and diabase dikes. The succession is unconformably overlain by the Goosly Lake basaltic to trachyandesitic volcanics that crop out in Riddeck Creek and farther south. Mineralization on the property is mainly restricted to quartz-carbonate-barite-specularite epithermal veins, 1- to 2-m thick, that contain disseminated to locally massive pyrite, sphalerite, galena, chalcopyrite, tennantite, and argentian tetrahedrite. Native gold is present in minor amounts. The mineralized veins cut the amygdaloidal, fine-grained plagioclase-rich dikes (unit 6), and are cut by the series of dikes with bladed plagioclase crystals (unit 7). Both these dike types belong to the Ootsa Lake Group of Eocene age. The bladed feldspar porphyry dikes cut the amygdaloidal dikes, and both are intruded by the diabase dikes of the Endako Group volcanism of Eocene-Oligocene age. Structurally, the Silver Queen area is dominated by a gently north-to-northwest dipping homocline with no apparent folding; the sequence presumably has been tilted 20° to 30° from the horizontal by block faulting. Two prominent sets of faults displace this homoclinal sequence, cutting it into a series of fault panels trending in the northwest and northeast directions, respectively. The former predates or is contemporaneous with mineralization and is suggested by Leitch et al. (1990) to correlate with the Ootsa Lake Group Goosley Lake volcanics of Eocene, approximately 50 Ma age, whereas the latter is mainly postmineralization. Most of the mineralized veins and the dikes follow the northwest-trending faults, whereas veins are cut off and displaced by the northeast-trending set. The northwest-trending faults dip 60° to 80° to the northeast and become subvertical to the south. The northeast-trending system appears

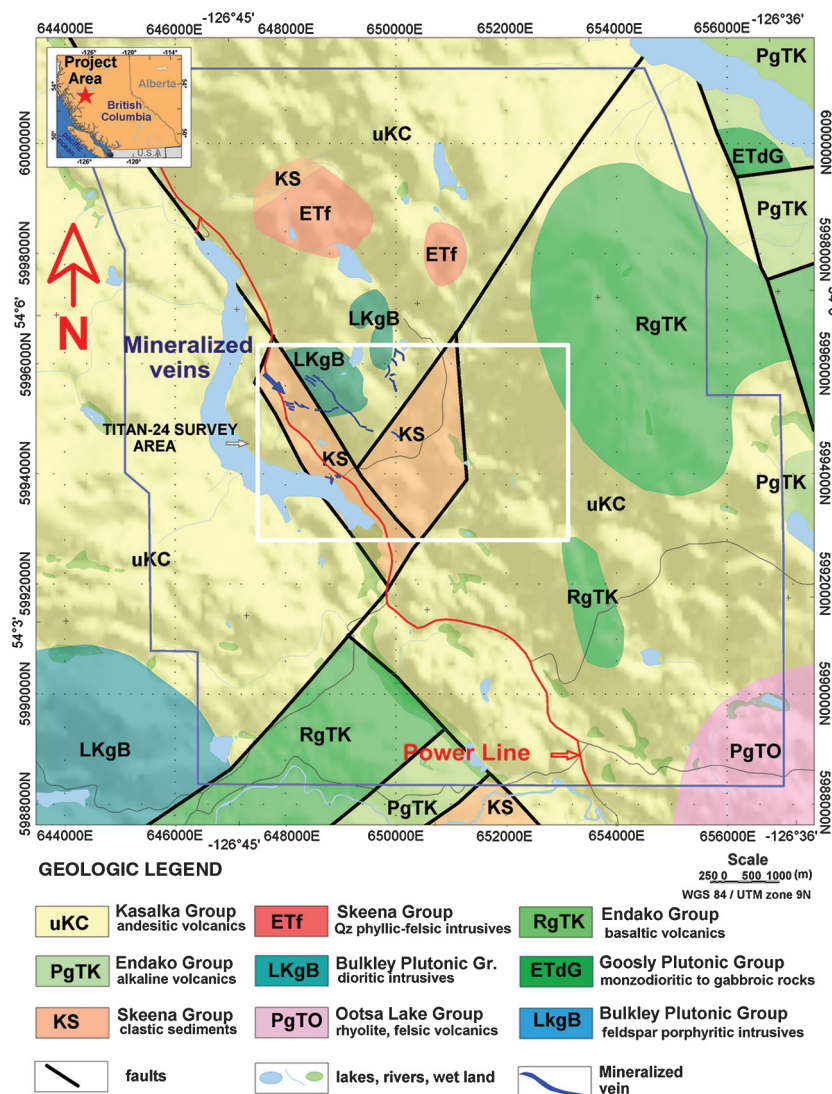


Figure 1. Regional geologic map of the Silver Queen area after McIntyre (1985) with shaded topography. The blue outlined area corresponds to the ZTEM survey. The area outlined in white is shown in detail in Figure 2 and corresponds to the TITAN-24 survey area.

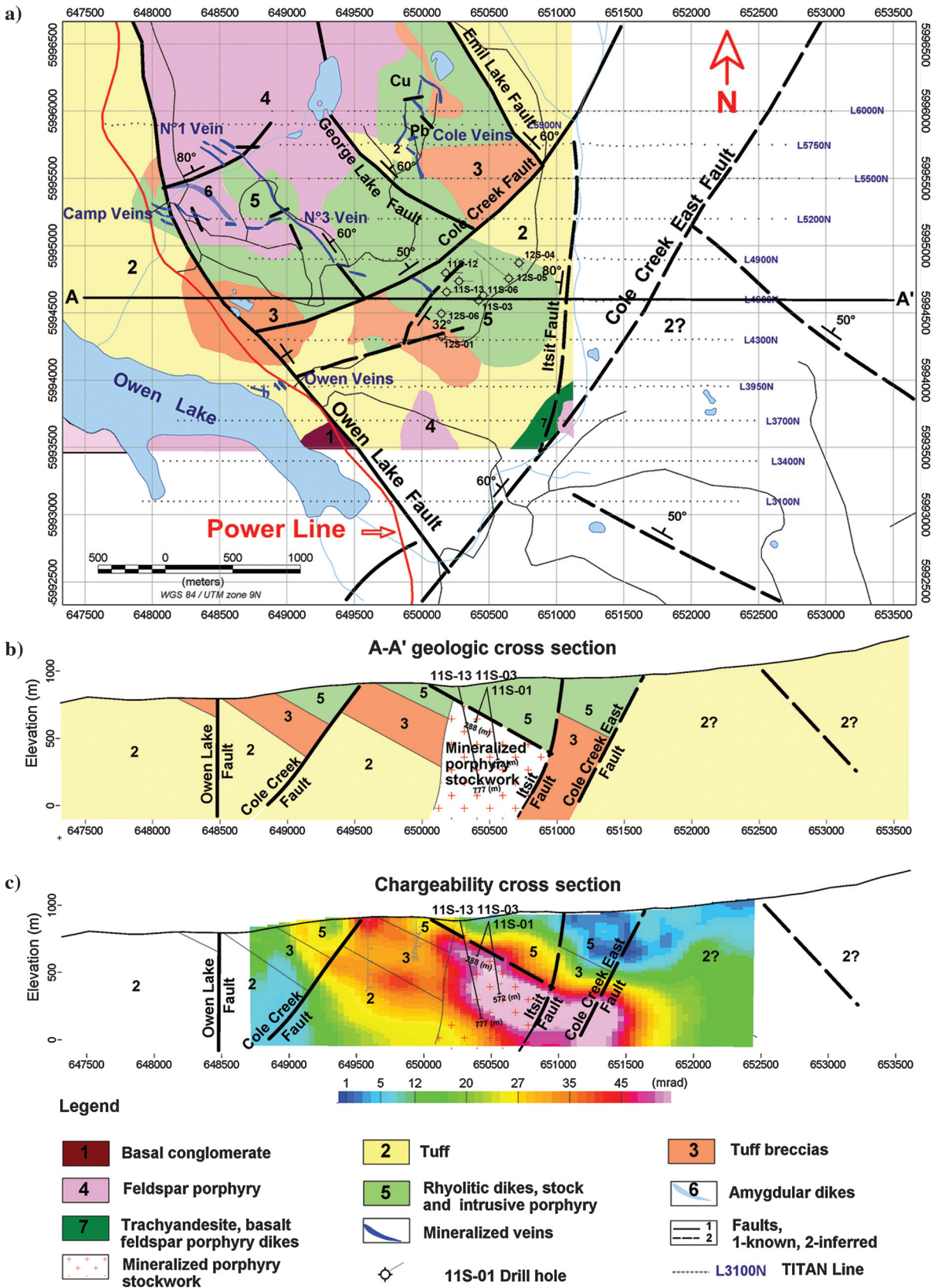


Figure 2. (a) Local geologic map of the Silver Queen after Leitch et al. (1990), (b) geologic cross section along line A-A', and (c) chargeability cross sectional view along line A-A' (extracted from the 3D chargeability inversion model).

to be dipping to the northwest at angles of 50° to 80° . Movement on the northwest-trending faults includes some dip slip, so that each successive panel to the east is upthrown, leading to a succession of deeper levels of exposures to the east. The sense of motion on some of the northeast-trending faults appears to be south side down, with a small component of sinistral shear (Leitch et al., 1990).

ZTEM survey results

ZTEM survey

A ZTEM helicopter-borne survey was flown over the Silver Queen area in May of 2011 by Geotech Ltd. The ZTEM system (Sattel et al., 2010) has proven to be a robust system due to improved signal processing and instrumentation compared to the older audio frequency magnetics (AFMAG) introduced by Ward (1959). The survey was flown at a nominal terrain clearance of 150 m along east–west traverses spaced at 200 m apart covering a total area of 10×12.5 km. The ZTEM system consisted of a moving horizontal coil of 7.4 m in diameter towed by a helicopter at a mean distance of 70 m underneath (Legault et al., 2012). The coil was used to measure the vertical magnetic component of the time-varying earth's magnetic field. In addition, a cesium magnetic sensor, towed at 55 m below the helicopter, was used to measure the static component of the earth's total

magnetic field. The ZTEM system requires 4 GPS units; one located on the helicopter tail boom for helicopter positioning and navigation, and a set of three located on the towed coil to monitor the attitude of the coil and to calculate the tilt of the coil away from the vertical axis during the survey. The tilt information was used in the processing for the correction of the measured tipper components (Kuzmin et al., 2010). To measure the horizontal component of the EM field, a set of two orthogonal square coils (3.5×3.5 m) were used as the ground base station. The relation between the measured parameters is given by Holtham and Oldenburg (2008, 2011)

$$H_z(r) = T_{zx}(r, r_0)H_x(r_0) + T_{zy}(r, r_0)H_y(r_0), \quad (1)$$

where H_z is the vertical component of the magnetic field measured in the center of the moving coil located at r ; H_x and H_y are the horizontal orthogonal components of the magnetic field measured at the ground base station located at r_0 ; and T_{zx} , T_{zy} are the tipper transfer functions defined by Holtham and Oldenburg (2011);

$$\begin{pmatrix} H_z^{(1)}(r) \\ H_z^{(2)}(r) \end{pmatrix} = \begin{pmatrix} H_x^{(1)}(r_0) & H_y^{(1)}(r_0) \\ H_x^{(2)}(r_0) & H_y^{(2)}(r_0) \end{pmatrix} \begin{pmatrix} T_{zx} \\ T_{zy} \end{pmatrix}, \quad (2)$$

where the superscripts (1) and (2) refer to the source magnetic field polarization in the x and y directions, respectively.

The airborne EM data were recorded at a sampling rate of 2000 Hz, whereas the magnetic data were sampled at 0.2 Hz. The ZTEM data were processed by Geotech Ltd. (Kowalczyk and van Kooten, 2011) and consisted mainly of calculating the x and y tipper components (T_{zx} and T_{zy}) according to equation 2 and applying the attitude correction to the measured data (Legault et al., 2012). The data were then presented as unrotated and rotated in-phase and quadrature components and tipper divergence at six frequencies ranging from 30 to 720 Hz (Legault et al., 2012).

When acquiring the magnetic data, a ground base station was used to record the diurnal variations of the earth's magnetic field. The measured magnetic data were corrected for the diurnal variation and reduced to the magnetic pole after the International Geomagnetic Reference Field removal (Telford et al., 1990).

Magnetic interpretation

Figure 3 depicts the reduced-to-the-pole residual magnetic anomaly including elements of structural and lithological interpretation inferred from the analysis

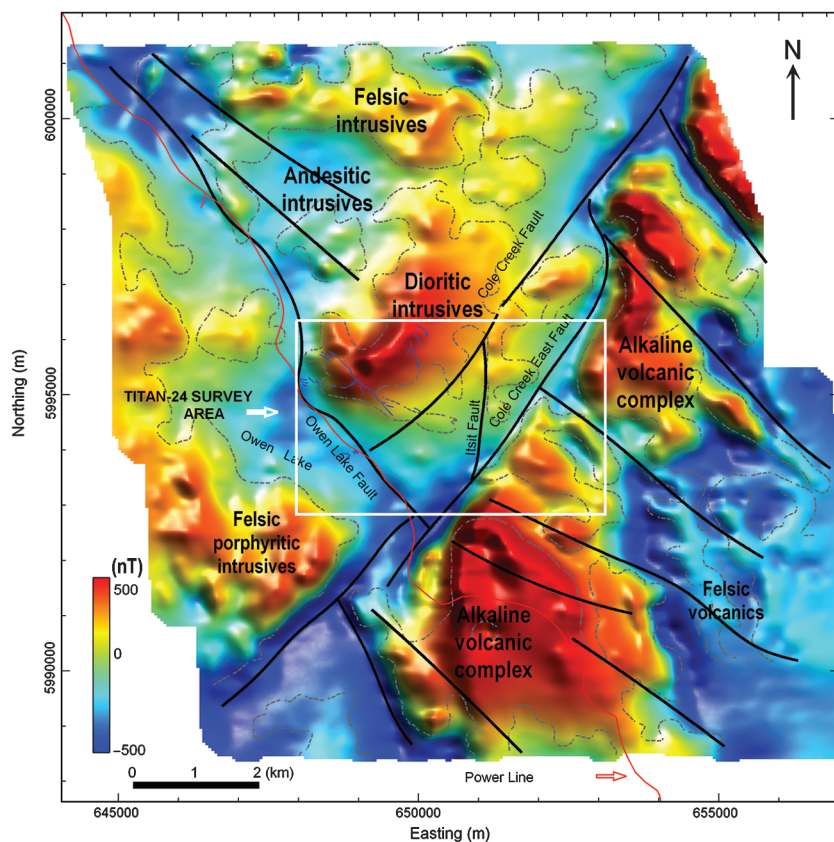


Figure 3. Color-shaded reduced-to-the-pole magnetic anomaly image including interpretation. The location of a power line is shown in red. The white rectangle indicates the TITAN-24 survey area.

of the data. It clearly highlights that areas of magnetic high in excess of 500 nT are associated with dioritic intrusives that host the mineralized veins occurring in the central area and with alkaline volcanics that are dominating the eastern and southern parts. Zones of moderate-to-moderately weak magnetic response observed in the north and west of the area appear to correspond to felsic rocks including intrusives and porphyritic intrusives. On the other hand, the wide zone of magnetic low observed in the southeast is likely attributed to altered felsic volcanic rocks. The well-defined northwest- and northeast-trending lineaments of magnetic low are attributed to known and inferred faults that are affecting the entire area. The low magnetic response associated with the fault zones is suggested to be caused by alteration and brecciation zones occurring along these faults and probably reflecting magnetite destruction. The plotted boundaries were inferred from enhancement filtering techniques using ZS-edge and ZS-block filter groups (Shi and Butt, 2004). The block and edge filters being linear- and derivative-based filters utilizing a combination of derivative and amplitude compression techniques to transform the magnetic data into regions similar to image classification analysis whose edges are sharply defined and whose amplitudes have a reduced range in comparison to the original magnetic data. These filters have been extensively used for source edge detection and lithological categorization from airborne magnetic data (Armstrong and Rodeghiero, 2006).

The 3D magnetic susceptibility model illustrated in Figure 4 was calculated using the MAG3D code (Li and Oldenburg, 1996). The model highlights the main geologic features composed essentially of intrusive and volcanic structures occurring within the Silver Queen area. The 3D model indicates clearly that recovered features exhibiting high magnetic susceptibility are associated with the dioritic intrusion occurring in the central area and the alkaline volcanic complex present in the east and south of the area. The 3D model also indicates that the Silver Queen mineralized vein system is hosted in the dioritic intrusive body. No magnetic rocks are, however, detected in the central area located at the intersection between the northwest and the northeast trending fault systems. This area may correspond to intense alteration and brecciation and therefore, represents a favorable zone, where porphyry-style mineralization is more likely to occur.

ZTEM interpretation

The ZTEM data are usually presented as profiles or gridded data of the x - and

y -components of the tipper transfer functions for the inphase (real) and quadrature (imaginary) components at each frequency. Based on a synthetic model study, Becken (2000) shows that the tipper transfer functions exhibit a single peak over contacts presenting resistivity contrasts and a crossover over thin conductors. This situation makes difficult the analysis of the tipper data without any a priori information about the geologic patterns. Moreover, the x - and y -components can behave differently, adding more complication in the analysis of the tipper maps as shown in Figure 5 (the 30 Hz gridded tipper data). Recently, Lo and Zang (2008) show that the ZTEM tipper transfer functions can be transformed in an easy way for the qualitative analysis purposes of profile and gridded data by the means of the divergence operator first applied by Pedersen (1998) to VLF data and defined by

$$\nabla \cdot \mathbf{T} = \text{div} \mathbf{T} = \text{div}(T_{zx}, T_{zy}) = \left(\frac{\partial T_{zx}}{\partial x} \right) + \left(\frac{\partial T_{zy}}{\partial y} \right). \quad (3)$$

The main advantage of using equation 3 is to transform the crossover anomaly type into a single peak anomaly located above the conductor. This offers a powerful resistivity mapping tool especially for detecting subvertical dike-like conductors; however, the divergence being a horizontal derivative operator

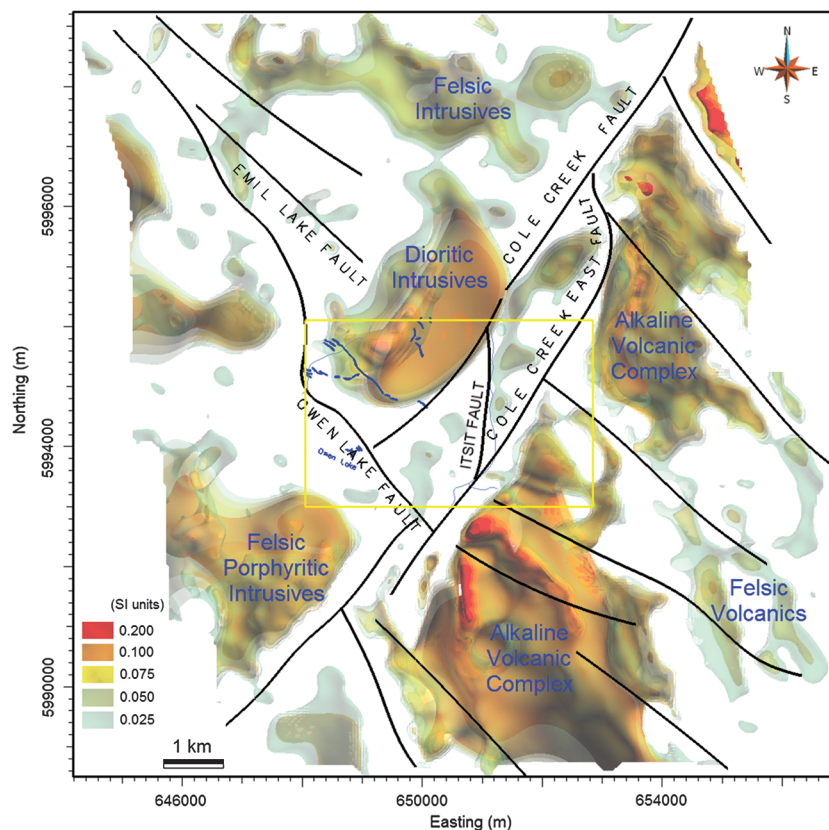


Figure 4. Three-dimensional magnetic susceptibility model isosurfaces (view from top). The yellow rectangle indicates the TITAN-24 survey area.

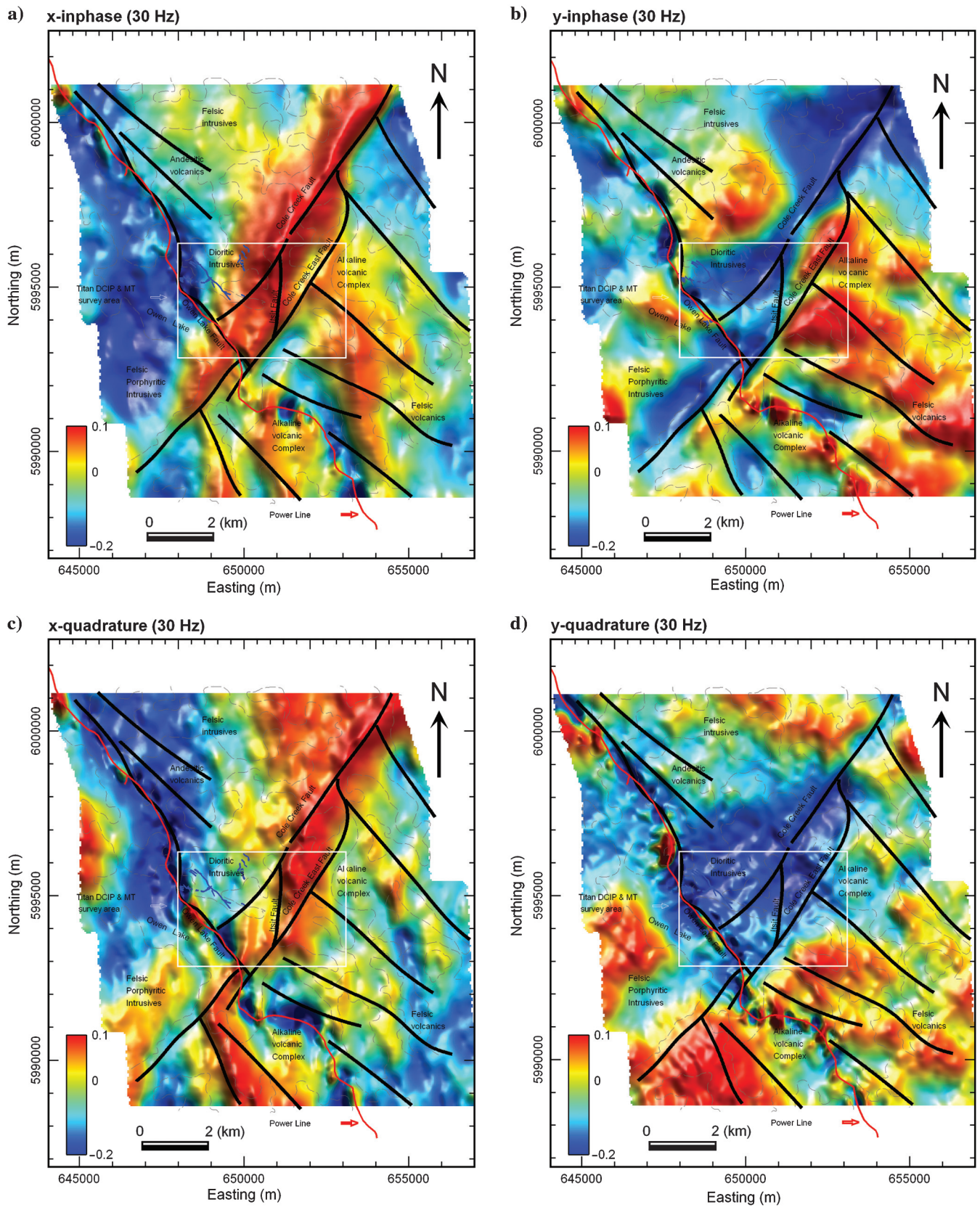


Figure 5. Color-shaded tipper transfer function images for the 30-Hz frequency; (a) inphase x -component, (b) inphase y -component, (c) quadrature x -component, and (d) quadrature y -component.

emphasizes the short wavelength component compared with the long wavelength component associated with deep-seated structures. It can also amplify the short wavelength noise component in the data. Over contacts, the divergence transforms the single peak anomaly type into a crossover.

Figure 6 depicts the tipper divergence of the real component and corresponding to four frequencies, 720, 180, 45, and 30 Hz. The overall tipper data correlate well with known geology by highlighting the major faults and zones of brecciation, particularly the north-east-trending Cole Creek fault and delineating the geologic structures representing resistivity contrasts. In addition, the analysis of the data allowed the detection of a new north-south trending fault in the central area, denoted as the Itsit fault indicated on maps in Figures 4–7. The tipper divergence exhibits short wavelength lineaments of negative sign over the conductive faults and brecciation zones. It is observed that the dioritic and porphyritic intrusives, being resistive formations, exhibit high values of the tipper divergence, whereas the volcanic rocks including andesitic, felsic, and alkaline rocks exhibit a moderate tipper divergence response. The data appear to be significantly affected by cultural noise induced by a power line running from the southeast to the northwest along the western half of the survey area. The noise effect is more significant at higher frequencies and tends to attenuate at lower frequencies. Kowalczyk and van Kooten (2011) computed the 3D conductivity structure of the subsurface from the ZTEM survey using the 3D MT inversion algorithm (Holtham and Oldenburg, 2008, 2011) including a range of six frequencies. The noisy data induced by the power line and included mainly in the high-frequency component were filtered and removed prior to the inversion. The 3D model shown in Figure 7 has identified one broad oval-shaped resistive body located in the central area, and this is most likely attributed to a dioritic intrusion that hosts the Silver Queen mineralized veins. Also evident are two resistive bodies of smaller size located in the north and southwest of the property and associated with felsic intrusives and felsic porphyritic intrusives, respectively. The east and southeast areas are predominated by a large conductive zone bound to the west by the northeast trending Cole Creek faulting system. The conductive zone appears to be associated with a thick package of overburden formations and the alkaline volcanic complex encountered in the southern portion of the property. It is also noticeable that most of the conductive lineaments identified east and southeast of the area are linked to conductive faults including alteration and brecciation zones. In addition, the 3D inversion results allowed identifying a moderately conductive zone of a small size, located in the south end of the broad resistive dioritic intrusive and close to the Silver Queen vein system, in the center of the of the TITAN-24 survey area as shown on the map in Figure 7.

TITAN-24 DCIP/MT survey results

TITAN-24 survey

A TITAN-24 DCIP and MT survey was carried out by Quantec Geoscience Ltd. over the central area of Silver Queen as a follow-up to the previous airborne geophysical survey and particularly to determine the nature of the small conductor detected in the central area occurring at the intersection between the northeast and northwest trending faults to the west of the Itsit fault shown on the map in Figure 7. The DCIP and MT survey was conducted in two phases (2011 and 2012) and covered a total area of 5.5×3.5 km consisting of 13 east-west lines each of 3.6 km in length, and spaced at 250 m apart. Intrinsic to the acquisition of the DCIP data when using a distributed array system and a pole-dipole array configuration like the TITAN-24, the transmitter-leading and transmitter-lagging data are collected simultaneously. Data collection was further enhanced by using inline and crossline receiver dipoles of 150 m in length. The induced polarization data were processed using a robust processing technique involving time series stacking, robust statistics, current waveform deconvolution, digital filtering (Kingman et al., 2007; Eaton et al., 2010), and spectral model decay-curve fitting using the Halverson-Wait model (Halverson et al., 1981). The MT survey makes use of the same distributed acquisition system as the DCIP data to acquire the horizontal components of the naturally varying telluric electric field. The horizontal components (x and y) of the magnetic field were measured overnight using a set of two horizontal and orthogonal induction coils. In addition, a remote reference site, synchronized by GPS clock, was used during the MT survey. The data were collected over a frequency range of 10 kHz to 0.01 Hz, and were processed using simple and robust processing techniques using time series sampling, stacking and filtering, noise rejection, digital filtering, coherence sorting, and spectral density calculations (Egbert, 1997; Simpson and Bahr, 2005).

3D inversion results

The DCIP data were first edited and filtered, and then inverted using 2D and 3D inversion techniques using UBC codes (Oldenburg and Li, 1994; Li and Oldenburg, 2000). The 2D inversion yields resistivity and chargeability distributions as a function of depth along the surveyed lines, whereas the 3D inversion computes a 3D volume distribution of resistivity and chargeability in the subsurface of the survey area. The 3D DC resistivity code is based upon the minimization of an objective function subjected to misfit and boundary criteria, and the 3D IP model is computed on the basis of the recovered 3D conductivity model and the sensitivity matrix using a linearized approach (Li and Oldenburg, 2000). A discretized 3D mesh of $50 \times 50 \times 25$ m cell size was used to construct the 3D model and a homogeneous half-space was used as an initial model. The MT data were inverted using the 2D RLM code based on the finite-difference algorithm (Rodi and Mackie,

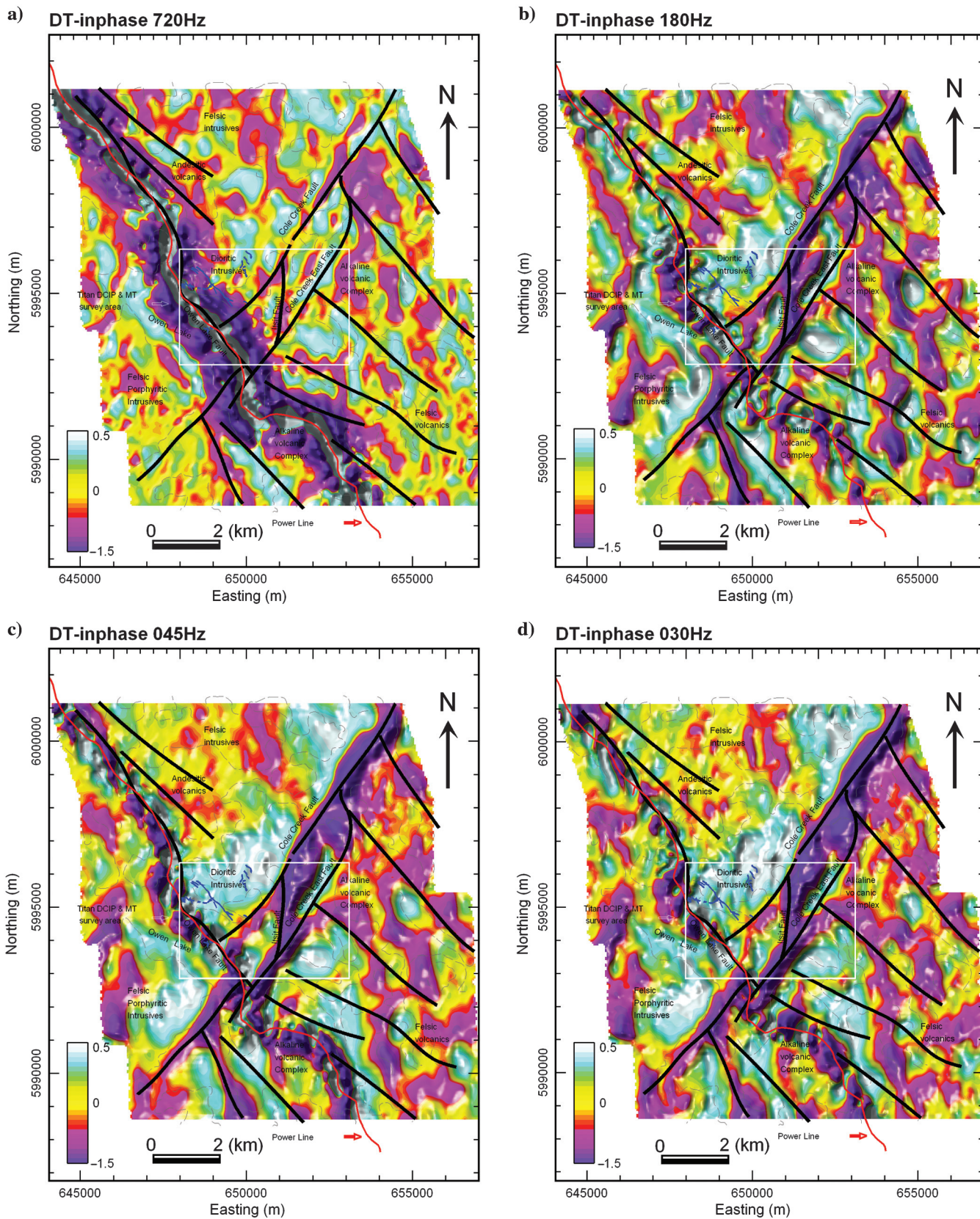


Figure 6. Color-shaded divergence of the inphase tipper transfer functions; (a) 720, (b) 180, (c) 45, and (d) 30 Hz.

2001), and the 3D MT parallelized code (Siripunvaraporn et al., 2005; Siripunvaraporn and Egbert, 2009) based on data space Occam's inversion. While the 2D MT code requires the definition of the transverse electric and transverse magnetic modes prior to the inversion, Siripunvaraporn (2012) mentioned the advantage of using the 3D versus 2D inversion with the main benefit that the strike analysis and dimensionality need not to be assumed or known prior to the 3D inversion. A total of 250 MT sites and 19 frequencies spanning the range of 10 kHz to 0.01 Hz with three frequencies per decade were used in the 3D inversion. A discretized 3D mesh of fixed 50×50 m cell size horizontally and variable size vertically starting from 25 m and increasing gradually with an expansion factor of 1.4 was used to build the starting model, which consists of a homogeneous half-space model of 100 ohm-m including the topography. The air layer was assigned a resistivity value of 10^8 ohm-m. The inverted parameters are the impedances defined by equation 4 (Vozoff, 1972)

$$\begin{pmatrix} E_x \\ E_y \end{pmatrix} = \begin{pmatrix} Z_{xx} & Z_{xy} \\ Z_{yx} & Z_{yy} \end{pmatrix} \begin{pmatrix} H_x \\ H_y \end{pmatrix}, \quad (4)$$

where Z_{ij} denotes the impedance tensor, E_x and E_y are the electric field components measured in the x - and y -directions, respectively, and H_x and H_y are the horizontal magnetic field measured in the x - and y -directions, respectively.

Figure 8 depicts the 3D resistivity and 3D chargeability models with the recent drillhole plots showing the copper assays. The 3D chargeability model highlights a strong chargeable feature roughly oriented in the northeast direction and appears to be bound to the northwest by the Cole Creek fault and to the south and northeast by the Cole Creek East fault. This feature is composed of a main core of 1.5×1 km in size trending in the north-northeast direction and surrounded by three other features of smaller size. The whole chargeable feature appears to be plunging southeastwards with the top being located in the west at the intersection of the Owen Lake and Cole Creek faults. It appears to be coincident with a northwest-trending zone of resistivity low of less than 10 ohm-m that plunges southeastwards. The core has a resistivity of less than 1 ohm-m and occurs at the intersection of Cole Creek and George Lake faults. Initially, this feature was suggested to be linked to a significant alteration zone with propylitic and pyritic mineralization.

However, upon completion of the first phase of the TITAN-24 survey, the target was drilled in the fall of 2011 and significant sulphides mineralization associated with a deep-seated porphyry stockwork was intercepted (Bournas et al., 2012). The deepest drillhole ended in mineralization at 777 m grading an average of 0.5% copper over 250 m and more importantly, revealed that the mineralization is open at depth (Hutter, 2011, 2012).

Upon completion of the second phase of the TITAN-24 DCIP and MT survey in 2012, the 3D DCIP and MT inversion results were assessed with the purpose to map and delineate the mineralized stockwork area to better guide further drilling. The results of the 3D DCIP and MT inversion results confirmed the existence of a significant deep-seated stockwork mineralized body, named Itsit, located southeast of the known vein system. These mineralized veins are suggested to extend into a deeper, larger stockwork body centered between the Cole Creek fault and the Cole Creek East fault and appears to be cut by the newly identified Itsit north-south trending fault. More recently, drilling performed in late of 2012 and early 2013 confirmed the presence of copper and molybdenum mineralization at depths varying from 250 m to approximately 1000 m (E. Clements, personal communication, 2013). Due to the significant size in horizontal and vertical

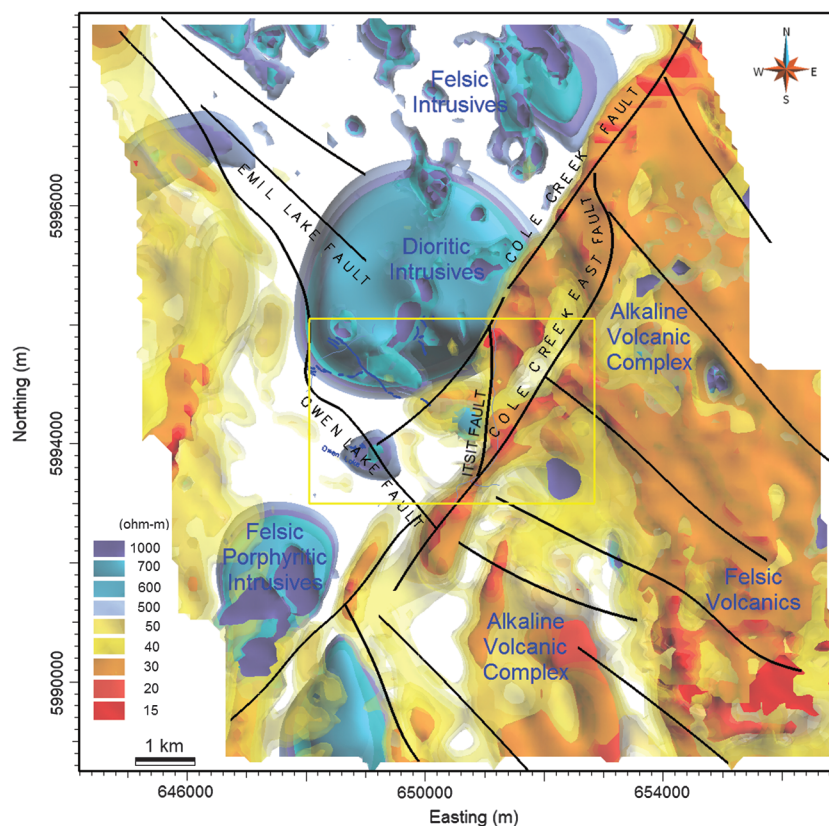


Figure 7. Three-dimensional ZTEM resistivity model isosurfaces (view from top). The yellow rectangle indicates the TITAN-24 survey area.

directions of the discovered stockwork porphyry, more drilling is needed to define areas of higher-grade mineralization.

The 3D MT model presented in Figure 9 as stacked vertical slices and resistivity shells depicts a deep-seated and broad conductive zone of approximately 2.5×1.5 km in size and elongated in the northwest direction with significant extension in the down-dip direction. The shallow conductive layer that dominates the eastern part is attributed to altered volcanics. In the horizontal plan, the core of the deep-seated anomalous feature occurs in the center of a triangular area formed by the Cole Creek fault, Owen Lake fault, and Itsit fault. This MT conductive feature appears of greater size when compared with the conductor recovered from the 3D DC inversion and also appears as shifted further to the south. This may be explained by the change of the shape and the dip of the conductor as depth increases. The aim of the MT inversion was to provide insights at

greater depths exceeding the depth of investigation of the DCIP technique.

The MT conductor was recently drilled and the results revealed its association with a significant alteration zone hosting stockwork porphyry mineralization extending from the near surface to a depth of up to 800 m with mineralization remaining open at depth (Hutter, 2012).

Discussions

A new significant polymetallic porphyry stockwork has been recently discovered within the Silver Queen property following the ZTEM and deep-penetrating TITAN-24 DCIP and MT surveys and the 3D inversion results of the data.

The 3D inversion results suggest that the porphyry body exhibits a strong chargeability response and low resistivity signature. The inferred feature has an irregular shape within a horizontal plan area of approximately

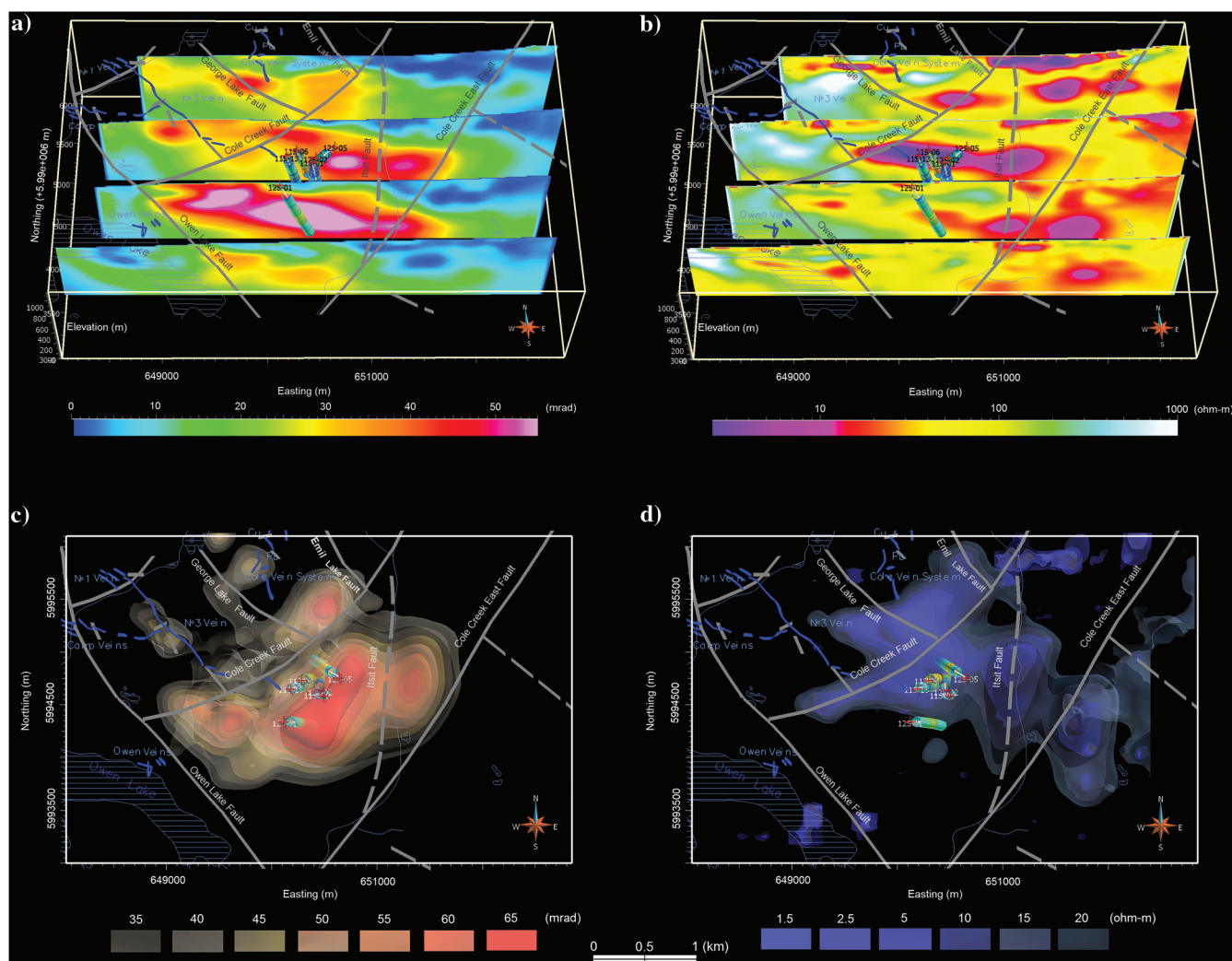


Figure 8. Three-dimensional inversion results of the TITAN-24 DCIP data: (a) vertical slices extracted from the 3D IP model (perspective view looking north), (b) vertical slices extracted from the 3D DC resistivity model (perspective view looking north), (c) chargeability isosurfaces (view looking down), and (d) DC resistivity isosurfaces (view looking down). Drillhole plots showing the copper assays and geologic faults and mineralized veins are included.

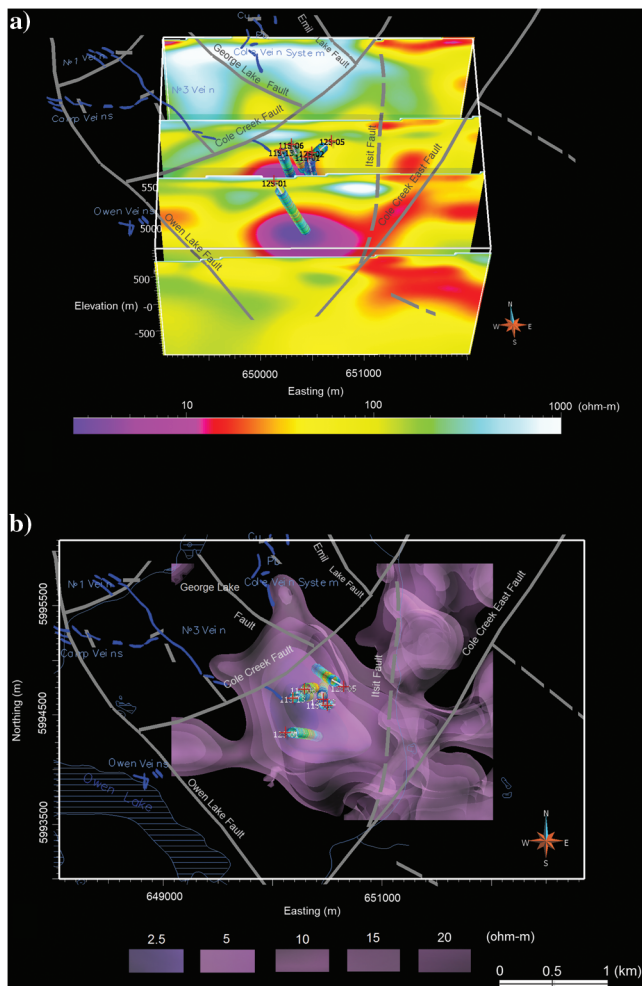


Figure 9. Three-dimensional inversion results of the TITAN-24 MT data: a) vertical slices extracted from the 3D MT resistivity model (perspective view looking north), and b) MT resistivity isosurfaces (view looking down). Drillhole plots showing the copper assays and geologic faults and mineralized veins are included.

2.5 × 1.5 km in size. A significant extension of the porphyry stockwork in the down-dip direction estimated as greater than 1 km is inferred from the 3D MT inversion results. The porphyry body is trending northeastwards and plunging to the southeast. Copper, gold, and molybdenum mineralization to a depth of over 800 m was confirmed by the 2011 and 2012 drilling campaigns. The porphyry system may represent a significant potential for economic polymetallic mineralization within the Silver Queen area. To date, only a few drillholes were completed to test the 3D DCIP and MT results and further drilling programs are required to identify zones of higher ore grade, thus increasing the potential of the discovered deposit.

Conclusions

A helicopter-borne ZTEM and magnetic survey flown over the Silver Queen polymetallic mineralized area revealed it is a very powerful tool that helped understand

the structural and lithological setting of the area. The 3D ZTEM inversion results were particularly useful in delineating one favorable area for further follow-up using ground DCIP and MT surveys by using the TITAN-24 system.

The 3D inversion results of the TITAN-24 DCIP and MT data led to the discovery of a significant stockwork mineralized zone confirmed by the recent drilling campaigns.

Acknowledgments

The authors thank New Nadina Explorations Ltd. for permission to publish these results. They are particularly thankful to Yonghe Sun, Ran Zhang, Giumin Liu, and another anonymous reviewer for their suggestions and very constructive comments to improve the overall quality of the manuscript. Special thanks to Richard Smith of Laurentian University for valuable discussions and comments.

References

- Armstrong, M., and A. Rodeghiero, 2006, Airborne geophysical techniques, *in* N. Aziz, ed., Coal 2006: Coal Operators' Conference, University of Wollongong & the Australasian Institute of Mining and Metallurgy, 113–131.
- Becken, M., 2000, Interpretation of magnetic transfer functions from airborne tensor-VLF measurements: M.S. thesis, Technical University of Berlin.
- Bournas, N., R. Hearst, and E. Clements, 2012, Silver Queen, a new stockwork porphyry discovery using the TITAN 24 DCIP and MT: 82nd Annual International Meeting, SEG, Expanded Abstracts, doi: [10.1190/segam2012-0254.1](https://doi.org/10.1190/segam2012-0254.1).
- Eaton, P., B. Anderson, S. Queen, I. Mackenzie, and D. Wynn, 2010, NEWDAS—the Newmont distributed IP data acquisition system: 80th Annual International Meeting, SEG, Expanded Abstracts, 1768–1772.
- Egbert, G. D., 1997, Robust multiple-station magnetotelluric data processing: *Geophysical Journal International*, **130**, 475–496, doi: [10.1111/j.1365-246X.1997.tb05663.x](https://doi.org/10.1111/j.1365-246X.1997.tb05663.x).
- Halverson, M. O., W. G. Zinn, E. O. McAlister, R. Ellis, and W. C. Yates, 1981, Assessment of results of broad-band spectral IP field test, *in* J. S. Summer, ed., *Advances in induced polarization and complex resistivity*: University of Arizona, 295–346.
- Holtham, E., and D. W. Oldenburg, 2008, Three-dimensional forward modeling and inversion of Z-TEM data: 78th Annual International Meeting, SEG, Expanded Abstracts, 564–568.
- Holtham, E., and D. W. Oldenburg, 2011, Large-scale inversion of ZTEM data: Presented at the International Workshop on Gravity, Electrical & Magnetic Methods and their Applications.
- Hutter, J., 2011, Significant intersections of porphyry-style mineralization encountered, Greenwood British Columbia, <http://nadina.com/properties/silver-queen/128>, accessed 19 October 2011.

- Hutter, J., 2012, New Nadina increases size of “TTIST” copper-Moly-Gold Porphyry, <http://nadina.com/news/2012-news-releases/133-new-nadina-increases-size-of-its-it-copper-moly-gold-porphyry->, accessed 28 March 2012.
- Kingman, J. E. E., J. G. Donohue, and T. J. Ritchie, 2007, Distributed acquisition in electrical geophysical systems: *Proceedings of Exploration 07*, 425–432.
- Kowalczyk, P. L., and P. B. M. van Kooten, 2011, ZTEM data inversion and interpretation using the UBC-GIF MTinv3D code: A case history at the Silver Queen project, British Columbia: Presented at the 22nd Geophysical Conference and Exhibition, ASEG.
- Kuzmin, P. V., G. Borel, E. B. Morrison, and J. Dodds, 2010, Geophysical prospecting using rotationally invariant parameters of natural electromagnetic fields: U.S. Patent 8,289,023.
- Legault, J. M., G. A. Wilson, A. V. Gribenko, M. S. Zhdanov, S. Zhao, and K. Fisk, 2012, An overview of the ZTEM and AirMt airborne electromagnetic systems: A case study from the Nebo-Babel Ni-Cu-PGE deposit, West Musgrave, Western Australia: *Preview*, **158**, 26–32.
- Leitch, C. H. B., C. T. Hood, X. L. Cheng, and A. J. Sinclair, 1990, Geology of the Silver Queen area: British Columbia Geological Survey, *Geological Fieldwork*, **1989**, 288–295.
- Li, Y., and D. W. Oldenburg, 1996, 3-D inversion of magnetic data: *Geophysics*, **61**, 394–408, doi: [10.1190/1.1443968](https://doi.org/10.1190/1.1443968).
- Li, Y., and D. W. Oldenburg, 2000, 3-D inversion of induced polarization data: *Geophysics*, **65**, 1931–1945, doi: [10.1190/1.1444877](https://doi.org/10.1190/1.1444877).
- Lo, B., and M. Zang, 2008, Numerical modeling of Z-TEM (airborne AFMAG) responses to guide exploration strategies: 78th Annual International Meeting, SEG, Expanded Abstracts, 1098–1102.
- McIntyre, D., 1985, Geology and mineral deposits of the Tahtsa Lake District, West-central British Columbia: British Columbia Ministry of Energy, Mines and Petroleum Resources, **75**.
- Oldenburg, D. W., and Y. Li, 1994, Inversion of induced polarization data: *Geophysics*, **59**, 1327–1341, doi: [10.1190/1.1443692](https://doi.org/10.1190/1.1443692).
- Pedersen, L. B., 1998, Tensor VLF measurements: Our first experiences: *Exploration Geophysics*, **29**, no. 2, 52–57, doi: [10.1071/EG998052](https://doi.org/10.1071/EG998052).
- Rodi, W., and R. L. Mackie, 2001, Non-linear conjugate gradient algorithm for 2-D magnetotelluric inversions: *Geophysics*, **66**, 174–187, doi: [10.1190/1.1444893](https://doi.org/10.1190/1.1444893).
- Sattel, D., K. Witherley, and M. Becken, 2010, A brief analysis of ZTEM data from the Forrestania test site, WA: ASEG, Extended Abstracts, 1–4.
- Shi, Z., and G. Butt, 2004, New enhancement filters for geological mapping: Presented at the 17th Geophysical Conference and Exhibition, ASEG.
- Simpson, F., and K. Bahr, 2005, *Practical magnetotellurics*: Cambridge University Press.
- Siripunvaraporn, W., 2012, Three-dimensional magnetotelluric inversion: An introductory guide for developers and users: *Surveys in Geophysics*, **33**, 5–27, doi: [10.1007/s10712-011-9122-6](https://doi.org/10.1007/s10712-011-9122-6).
- Siripunvaraporn, W., and G. Egbert, 2009, WSINV3DMT: Vertical magnetic field transfer function inversion and parallel implementation: *Physics of the Earth and Planetary Interiors*, **173**, 317–329, doi: [10.1016/j.pepi.2009.01.013](https://doi.org/10.1016/j.pepi.2009.01.013).
- Siripunvaraporn, W., G. Egbert, Y. Lenbury, and M. Uyeshima, 2005, Three-dimensional magnetotelluric inversion: Data-space method: *Physics of the Earth and Planetary Interiors*, **150**, 3–14, doi: [10.1016/j.pepi.2004.08.023](https://doi.org/10.1016/j.pepi.2004.08.023).
- Telford, W. M., L. P. Geldart, and R. E. Sheriff, 1990, *Applied geophysics*, 2nd ed.: Cambridge University Press.
- Vozoff, K., 1972, The magnetotelluric method in the exploration of sedimentary basins: *Geophysics*, **37**, 98–141, doi: [10.1190/1.1440255](https://doi.org/10.1190/1.1440255).
- Ward, S. H., 1959, AFMAG- airborne and ground: *Geophysics*, **24**, 761–787, doi: [10.1190/1.1438657](https://doi.org/10.1190/1.1438657).

Biographies and photos of the authors are not available.